

Carbazole-Linked Near-Infrared Aza-BODIPY Dyes as Triplet Sensitizers and Photoacoustic Contrast Agents for Deep-Tissue Imaging

Gawale, Yogesh; Adarsh, Nagappanpillai; Kalva, Sandeep Kumar; Joseph, Joshy; Pramanik, Manojit; Ramaiah, Danaboyina; Sekar, Nagaiyan

2017

Gawale, Y., Adarsh, N., Kalva, S. K., Joseph, J., Pramanik, M., Ramaiah, D., et al. (2017). Carbazole-Linked Near-Infrared Aza-BODIPY Dyes as Triplet Sensitizers and Photoacoustic Contrast Agents for Deep-Tissue Imaging. *Chemistry - A European Journal*, 23(27), 6570-6578.

<https://hdl.handle.net/10356/83068>

<https://doi.org/10.1002/chem.201605702>

© 2017 Wiley-VCH Verlag GmbH & Co. KGaA, Weinheim. This is the author created version of a work that has been peer reviewed and accepted for publication by *Chemistry - A European Journal*, Wiley-VCH Verlag GmbH & Co. KGaA, Weinheim. It incorporates referee's comments but changes resulting from the publishing process, such as copyediting, structural formatting, may not be reflected in this document. The published version is available at: [<http://dx.doi.org/10.1002/chem.201605702>].

1 Carbazole Linked NIR Aza-BODIPY Dyes as Triplet Sensitizers 2 and Photoacoustic Contrast Agents for Deep Tissue Imaging

3 Yogesh Gawale^[a], Nagappanpillai Adarsh^[b], Sandeep Kumar Kalva^[c], Joshy Joseph^[b], Manojit
4 Pramanik^{[c]*}, Danaboyina Ramaiah^{[d]*} and Nagaiyan Sekar^{[a]*}

Abstract: Four novel *N*-ethylcarbazole linked aza-BODIPY dyes (**8a-b** and **9a-b**) were synthesized and characterized. The presence of *N*-ethylcarbazole moiety shifts their absorption and fluorescence spectra to the near-infrared region, ca. 650-730 nm, of electromagnetic spectra. These dyes possess strong molar absorptivity in the range of $3-4 \times 10^4 \text{ M}^{-1}\text{cm}^{-1}$ with low fluorescence quantum yields. The triplet excited state as well as singlet oxygen generation of these dyes were enhanced upon iodination at the core position. The core iodinated dyes **9a-b** showed excellent triplet quantum yield of ca. 90% and 75% with singlet oxygen generation efficiency of ca. 70% and 60% when compared to the parent dyes. The derivatives **8a-b** showed dual absorption profiles in contrast to the dyes **9a-b**, which has the characteristic absorption band of the aza-BODIPY dyes. The DFT calculations revealed the electron density spread over the iodine and dipyrromethene plane of the aza-BODIPYs, **9a-b**, whereas in **8a-b** the electron density distributed on carbazole ring as well as dipyrromethene plane of aza-BODIPY. The uniqueness of these aza-BODIPY systems is that they exhibit efficient triplet state quantum yields, high singlet oxygen generation yields and good photostability. Further we explored the photoacoustic (PA) characteristics of these aza-BODIPY dyes, and observed efficient PA signals for **8a** compared to blood serum with *in vitro* deep tissue imaging, thereby confirming its use as a promising photoacoustic contrast agent.

Introduction

There are four major reactive oxygen species (ROS) comprising superoxide (O_2^-), hydroxyl radical ($\cdot\text{OH}$), hydrogen peroxide (H_2O_2), and singlet oxygen $\text{O}_2(^1\Delta_g)$, but all these species show different level of activity and kinetics. The hydroxyl radical and singlet oxygen are more toxic and acutely lethal compared to superoxide and hydrogen peroxide. The generation of singlet

oxygen through photosensitization is one of the most utilized method in recent years.^[1] Due to the spin-allowed nature of the reactions, singlet oxygen exhibits high reactivity towards most of the organic molecules and thus it has the ability to interrupt the cellular functions in living organisms. Photodynamic therapy is based on the formation of reactive oxygen species (ROS), specifically singlet oxygen, upon activation of the photosensitizer by light.^[2] It damages the biological tissues by subsequent oxidation. Hence, the quantitative generation of singlet oxygen (Φ_{Δ}) is one of the important requirement of an efficient photosensitizer (PS)^[3]

Most of the photosensitizers used for the generation of singlet oxygen comprises of a common cyclic tetrapyrrolic structure, derived from porphyrins. Apart from this several non-porphyrinic systems reported in the literature to serve the purpose of singlet oxygen generation and these include methylene blue, Nile blue, Nile red, Rose bengal, chalcogenopyrylium salts, squaraine dyes etc.^[4] However, the drawbacks of such classes of PS are low molar absorption coefficients in the near infer-red (NIR) region and dark toxicity. An ideal PS should possess good stability and should have high absorption in the range of 600-800 nm, below which the light will be absorbed by different tissues and above which it does not provide energy to excite oxygen to its singlet state.^[5]

Recently, the chemistry of dipyrromethene ligands and their boron complexes (BODIPY) has attracted much attention due to their favorable photophysical properties such as intense absorption at long wavelength with high molar absorption coefficients ($\epsilon > 10^4 \text{ M}^{-1}\text{cm}^{-1}$), moderate to quantitative fluorescence quantum yields and chemical properties, which include tunability through substitution at different positions.^[6] Aza-dipyrromethenes and aza-BODIPY dyes were first described several years ago as blue pigments, but now are rapidly emerging as a class with desirable near infrared photophysical properties.^[7]

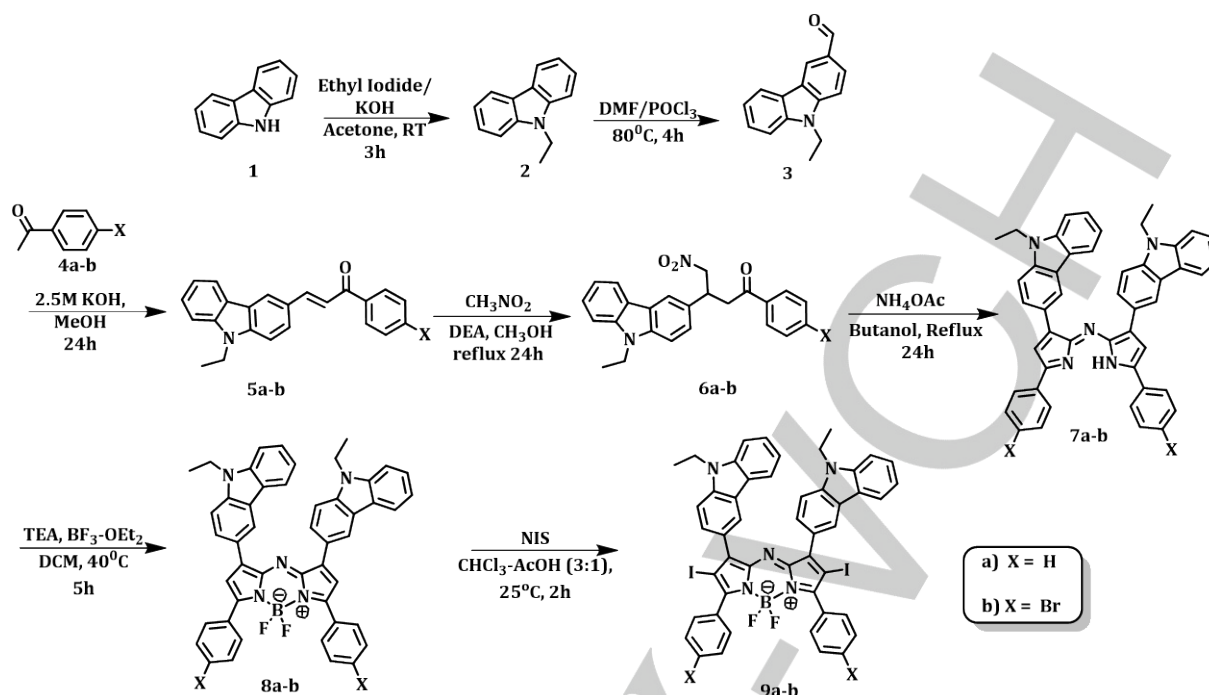
The strong absorption of light in the NIR region has also finds potential application of these dyes as photoacoustic (PA) contrast agent.^[8] PA imaging is gaining attention as an emerging deep tissue biomedical imaging modality that incorporates rich optical contrast and high ultrasound resolution. Due to this added advantage, PA imaging finds many applications in breast cancer imaging, brain imaging, tumour angiogenesis, molecular imaging, sentinel lymph node imaging, vascularisation monitoring and so on.^[9] Moreover, these contrast agents help in targeted PA imaging and molecular imaging with high contrast and sensitivity.^[10]

[a] Y. Gawale, Prof. N. Sekar
Dyestuff Technology Department,
Institute of Chemical Technology,
Matunga, Mumbai, 400 019, India,
n.sekar@ictmumbai.edu.in, nethi.sekar@gmail.com

[b] Dr. N. Adarsh, Dr. J. Joseph
Chemical Sciences and Technology Division
CSIR-National Institute for Interdisciplinary Science and
Technology, Thiruvananthapuram - 695 019, Kerala, India

[c] S. K. Kalva, Dr. M. Pramanik
School of Chemical and Biomedical Engineering
Nanyang Technological University
62 Nanyang Drive, Singapore 637459,
manojit@ntu.edu.sg

[d] Dr. D. Ramaiah
CSIR-North East Institute of Science and Technology,
Jorhat 785 006, Assam, India
d.ramaiah@gmail.com



Scheme 1: Synthetic route for the aza-BODIPY dyes **8a-b** and **9a-b**.

Herein, we designed a new series of carbazole linked aza-BODIPY derivatives with an objective of developing new and efficient photosensitizers and photoacoustic imaging agents that exhibit near infrared absorption in the range of ca. 600-800 nm. We synthesized a series of the *N*-ethylcarbazole linked aza-BODIPY dyes, characterised and have investigated their photophysical properties, triplet excited state and singlet oxygen generation efficiencies. The photoacoustic characteristics of these dyes were investigated and the derivative, **8a** was found to be efficient for *in vitro* deep tissue imaging application.

Results and Discussion

Synthesis and characterization: The synthetic strategy adopted for the synthesis of *N*-ethylcarbazole linked aza-BODIPY **8a-b** and **9a-b** using different acetophenone derivatives is shown in Scheme 1. The aza-BODIPY derivatives **8a-b** and **9a-b** were synthesized in a facile six step route starting from carbazole **1**. *N*-Ethylation of carbazole by ethyl iodide in acetonitrile yielded **2**, which upon Vilsmeier-Haack formylation gave the corresponding formyl derivative, **3** in good yield. Further, aldol condensation reaction between **3** and the acetophenone derivatives **4a-b** yielded the respective chalcones **5a-b**. The addition of nitromethane to the chalcone in presence of diethylamine gave the adducts **6a-b**, which upon refluxing with ammonium acetate in butanol for 20 h gave the corresponding aza-dipyromethenes **7a-b** as condensation products. The aza-dipyromethenes **7a-b** were subsequently converted to the targeted aza-BODIPY derivatives **8a-b** (35-40%) by reacting with borontrifluoride diethyletherate and

triethylamine at 40 °C in dichloromethane for 5 h. The controlled iodination of **9a-b** was carried out by modifying the reported procedures using NIS as the iodinating agent and achieved 60-65% yield.^[3a]

Absorption and fluorescence properties: *N*-Ethylcarbazole linked aza-BODIPY dyes, **8a-b** showed very distinct photophysical properties as compared to their iodinated derivatives, **9a-b**. The non-iodinated dyes **8a-b** showed dual absorption in the red region (610-720 nm) and having molar extinction coefficients 3.0 and $3.2 \times 10^4 \text{ M}^{-1}\text{cm}^{-1}$, (Figure S27, Supporting Information) respectively. Interestingly, for the core iodinated aza-BODIPY derivatives **9a-b**, we observed a single absorption profile with a maximum at ca. 645-655 nm (Figure 1A, S24, Supporting Information), with an enhanced molar absorptivity of ca. 3.7 and $4.1 \times 10^4 \text{ M}^{-1}\text{cm}^{-1}$, respectively. All these aza-BODIPY derivatives exhibited good solubility in common organic solvents such as CH_3CN , CHCl_3 , THF and DMSO.

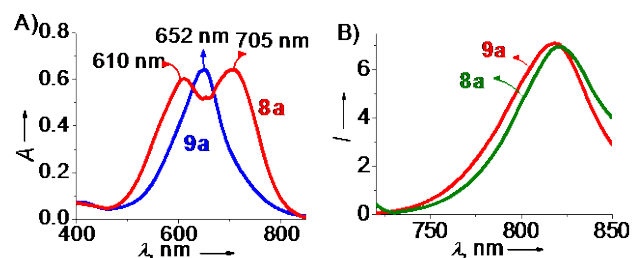


Figure 1: A) Absorption and B) fluorescence spectra of the representative aza-BODIPY derivatives **8a** and **9a** in acetonitrile (20 μM each).

Table 1. Summary of photophysical, electrochemical and theoretical parameters for the aza-BODIPY dyes **8a-b** and **9a-b**

Dyes	λ_{abs} (nm)	ϵ_{max} ($\text{M}^{-1}\text{cm}^{-1}$)	λ_{em} (nm)	$\Phi_f^{[a]}$	Stokes shift (cm^{-1})	E_{HOMO}		E_{LUMO}		E_{gap}		Triplet and singlet oxygen parameters		
						Experiment	Theory	Experiment	Theory	Experiment	Theory	$\Phi_T^{[b]}$	$\tau_T^{[c]}$	$\Phi_{\Delta}^{[d]}$
8a	705	3.0×10^4	818	0.22	1959.46	-5.322	-5.297	-3.86	-3.381	1.462	1.916	e	e	1
9a	653	3.7×10^4	815	0.03	3067.49	-5.343	-3.583	-3.899	-1.050	1.444	2.533	90	1.15	70
8b	723	3.2×10^4	820	0.03	1636.14	-4.082	-5.324	-2.69	-3.461	1.39	1.863	E	e	1
9b	649	4.1×10^4	830	0.32	3360.13	-4.16	-3.645	-2.67	-1.102	1.48	2.544	75	1.64	61

[a] Absolute quantum yield in % [b] Quantum yield of triplet state, were calculated by using the triplet-triplet energytransfer in % [c] Triplet state lifetime [d] Quantum yield of singlet oxygen, were quantified through scavenging of $^1\text{O}_2$ by DPBF [e] Triplet is not observed in Acetonitrile.

Figure 1B (Figure 26, Supporting Information) shows the emission spectra of the corresponding *N*-ethylcarbazole linked aza-BODIPY derivatives in acetonitrile. The aza-BODIPY derivatives **8a-b** showed emission in the region 815-825 nm with Stokes shifts of 113 nm and 97 nm, respectively. Interestingly, the core iodine substituted aza-BODIPY derivatives **9a-b**, also showed emission maxima in the region 815-830 nm marking large Stokes shifts values of 163 nm and 181 nm, respectively.

Determination of triplet excited state quantum yields

The transient intermediates such as triplet excited states involved in these systems were characterized and quantified through nanosecond laser flash photolysis. The time-resolved transient absorption spectra of the compounds were studied. Figure 2 shows the transient absorption spectra of **9a** in acetonitrile obtained after 355 nm laser excitation (10 ns, 50 mJ pulse). For the derivative **9a**, the transient absorption spectra has two peaks at 320 nm and 460 nm with a strong bleach in the region corresponding to its ground state absorption. The transient was characterized as triplet excited state using oxygen quenching experiments as reported previously.^[11, 6d] The triplet formed from **9a** within laser pulse, decayed by a first-order process with a lifetime value of 1.15 μs (Inset of Figure 2).

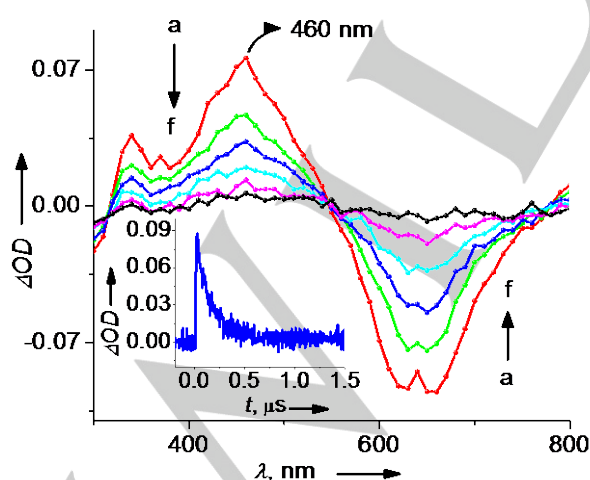


Figure 2: Transient absorption spectra of A) **9a** following 355 nm laser pulse excitation; time-resolved absorption spectra recorded at (a) 0.5, (b) 0.2 (c) 0.1 (d) 0.05, (e) 2 μs . Inset shows the decay of the transient at 460 nm.

In case of dye **9b**, similar transient absorption spectrum observed having bands at 320 nm and 460 nm formed upon the excitation with 355 nm laser (Figure S28, Supporting Information). Triplet quantum yields of **9a** and **9b** derivatives were determined using triplet-triplet energy transfer to β -carotene using tris(bipyridyl)ruthenium(II) complex as the reference (Table 1).^[7c, 12]

Quantification of singlet oxygen generation: Enhanced triplet quantum yields are favorable for the efficient generation of singlet oxygen and therefore we have examined the singlet oxygen generation efficiency of the derivatives **9a** and **9b** in acetonitrile. Quantum yields of singlet oxygen generation were determined by monitoring the photooxidation of 1,3-diphenylisobenzofuran (DPBF) through absorption spectroscopy.^[13] For this, a solution of the aza-BODIPY derivative and DPBF were irradiated using 630 nm long pass over a time period of 0-10 s and the decrease in the absorption band of (~10%) of DPBF at 409 nm was monitored (Figure 3A). Yields for the generation of singlet oxygen were calculated using the standard, Methylene Blue (MB), and by plotting the ΔOD of DPBF against the irradiation time (Figure 3B). The non-iodinated aza-dipyrromethenes **8a** and **8b** showed negligible singlet oxygen generation efficiency.

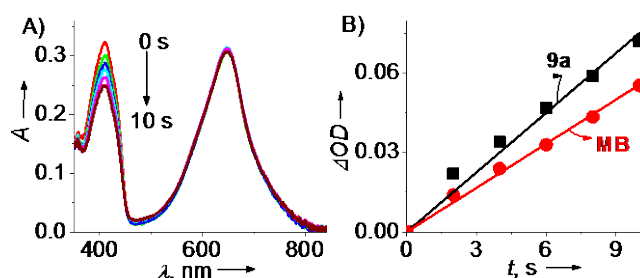


Figure 3: A) Absorption spectra of diphenylisobenzofuran (DPBF) upon irradiation in presence of **9a** from 0 to 10 s (recorded at 2 s interval) in ACN, B) straight line plot between the changes in absorption of DPBF with the irradiation time.

From the previous reports, it is clear that the tuning of singlet oxygen generation efficiencies of the aza-BODIPY derivatives can be achieved by suitably incorporating the heavier halogen atoms such as iodine and bromine at the core as well

1 as at the peripheral phenyl rings.^[3a] We have observed the
 2 similar effect for the carbazole linked aza-BODIPY dyes **8a-b**
 3 and **9a-b**. The aza-BODIPY derivative, **8a** showed negligible
 4 singlet oxygen generation efficiency while a slight improvement
 5 was observed with peripheral substitution with bromine as in **8b**
 6 (Table 1). On the other hand, a significant enhancement in
 7 singlet oxygen generation was observed upon iodination at core
 8 position (**9a**). To summarize, the derivatives **9a** and **9b**, having
 9 two iodine atoms at the core of the pyrrole exhibited singlet
 10 oxygen quantum yield of 70% and 60%, respectively (Figure 3,
 11 S29, Supporting Information) when compared to the standard
 12 MB ($\Phi_{\Delta} = 52\%$).^[14] The negligible changes in the absorption
 13 spectra after irradiating an oxygen saturated solution of these
 14 dyes for 2 h, indicates their photostability under these conditions.

15 **Electrochemical properties:** We have investigated the
 16 oxidation and reduction potentials of **8a-b** and **9a-b** using cyclic
 17 voltammetry and square wave voltammetry techniques in
 18 acetonitrile using 0.1 M TBAPF₆ as the supporting electrolyte.
 19 Acetonitrile solutions were purged with N₂ and scanned at a rate
 20 of 100 mV s⁻¹. The redox potentials were calculated using the
 21 potentials obtained from the square wave voltammograms
 22 (Figure S30, Supporting Information). Table 1 lists the calculated
 23 HOMO-LUMO energies of the compounds **8a-b** and **9a-b**. It can
 24 be seen that unlike ferrocene, which showed single oxidation
 25 wave at 0.38 V,^[15] all the aza-BODIPY derivatives exhibited two
 26 oxidation and two reduction waves in their cyclic
 27 voltammograms (CV). Incorporation of the iodo atom at core
 28 position of aza-BODIPY **8a** and **8b** has a negative effect on the
 29 oxidation potentials (E_{ox}). The dyes **8a** ($E_{ox} = 5.322$ V) and **8b**
 30 ($E_{ox} = 5.343$ V) possess higher oxidation potential as compared
 31 to **9a** ($E_{ox} = 4.082$ V) and **9b** ($E_{ox} = 4.16$ V), by 1.24 V and 1.18 V.
 32 This can be attributed to the presence of iodine atom at the core
 33 position, which leads to the rigidification of the core and hence
 34 the reduction processes become more feasible for the aza-
 35 BODIPY **8a** and **8b**. The HOMO values of the aza-BODIPY
 36 derivatives increases in the order **8b** < **8a** < **9b** < **9a**.

37 **Frontier molecular orbital energies.** The energy levels of
 38 the frontier molecular orbitals (FMOs), especially HOMO-1,
 39 HOMO, LUMO and their spatial distributions are useful to predict
 40 the behavior of the molecules in terms of their electronic
 41 structures, photophysical properties, and photostability. Herein
 42 we report the contour plots of the HOMO-1, HOMO and LUMO
 43 of dyes **8a**, **9a**, **8b** and **9b** in acetonitrile as shown in (Figure 4,
 44 S31, Supporting Information). These energy values were
 45 calculated by employing B3LYP/6-31G level of theory for aza-
 46 BODIPY **8a**, **8b**, **9a**, and **9b**. These states encompasses
 47 complex orbital contribution, beyond the crude HOMO-LUMO
 48 so that barely considering these two frontier orbitals would not
 49 provide accurate energy gap^[16, 61] and hence deviated more
 50 compared to the experimental energy gap. HOMO-1 orbital of
 51 dye **8a** and **8b** clearly indicate the electron density is situated
 52 more on the carbazole ring as compared to the aza-BODIPY
 53 core. Whereas, HOMO-1 orbital of dye **9a** and **9b** indicate the
 54 whole electron density is situated on pyrrole core towards iodine
 55 atom due to its heaviness. In the case of HOMO of dye **8a** and
 56 **8b**, the electron density is distributed almost uniformly over the
 57 entire chromophore. Interestingly, for the dyes **9a** and **9b**, unlike

for dyes **8a** and **8b**, the electron density in HOMO is localized
 only on the pyrrole position and the aza-BODIPY core.

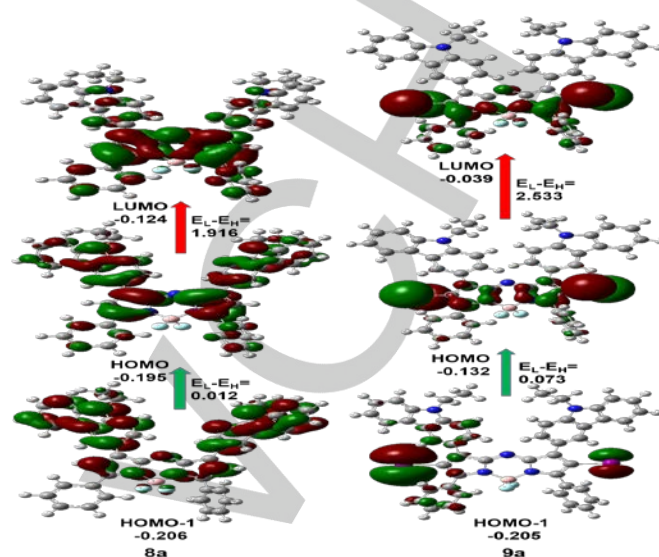


Figure 4: Energy level diagram containing the HOMO-1, HOMO and LUMO levels of **8a** and **9a** calculated at B3LYP/6-31g level.

DFT results suggested that iodination at the core position
 of aza-BODIPY affects the orientation of carbazole group at the
 peripheral position. The dihedral angle of **8a** (1c-2c-3c-4c)
 between the carbazole group and dipyrromethene plane is 21°,
 whereas the dihedral angle of **9a** increases to 41° (Figure 5).
 Similar observations noticed in case of aza-BODIPY **8b** and **9b**,
 in which the dihedral angle increased from 20° to 41°. Hence we
 have observed reasonable enhancement in band gap of
 iodinated derivatives **9a** and **9b** as compared to **8a** and **8b**.

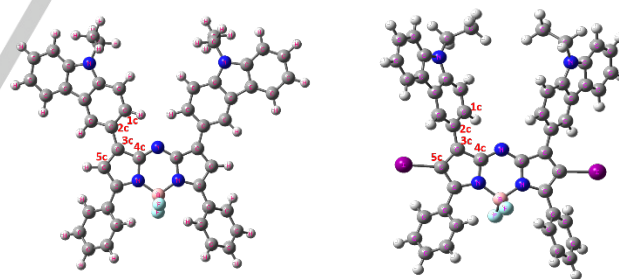


Figure 5: Optimized geometry of **8a** and **9a** at B3LYP/6-31g level.

Photoacoustic spectrum (PAS). According to the
 Kasha's rule,^[17] the non-radiative decay ($S_n \rightarrow S_1$) is responsible
 for the enhancement in PA signal, followed by the competition
 between radiative and non-radiative pathways for the $S_1 \rightarrow S_0$
 transition. An organic material having strong NIR absorption and
 long-lived S_1 excited state (life time of excited state) facilitating
 excited-state absorption is expected to produce an enhanced PA
 signal.^[18] We further attempted to understand the potential of
 aza-BODIPY dyes as molecular photoacoustic contrast agents
 in solution as well as in the tissue. We have initially performed
 the photoacoustic study on the aza-BODIPY dyes (**8a-b**, **9a-b**) in
 acetonitrile at a concentration of 30 μ M. The PA spectra were

measured in the wavelength range from ca. 670-970 nm with an interval of 5 nm. The PAS of each sample is compared to that of animal blood. Figure 6A (Fig. S32, Supporting Information) shows the PA spectrum of samples **8a-b**, **9a-b** dissolved in acetonitrile with respect to the PA spectrum of blood. Peak to peak normalized PA signal has been calculated at each wavelength.

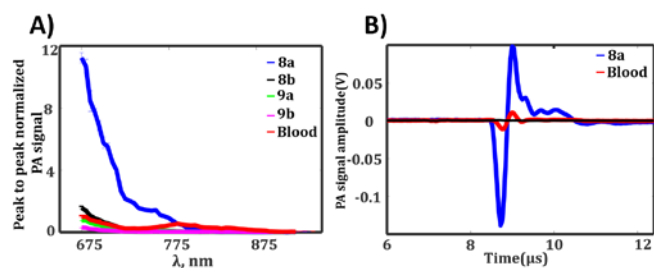


Figure 6: Photoacoustic spectra of aza-BODIPY dyes in acetonitrile (30μM). (A) PA spectra of **8a**, **8b**, **9a**, and **9b** in solvent ACN compared to that of blood. (B) PA signal comparison of sample **8a** in ACN with blood and water (control data) at 675nm.

The PA signal of dyes **8a** and **8b** are higher than that of blood compared to the rest of the samples at 675 nm. The PA signal of the core iodinated derivatives **9a-b** are much lower than that of blood which may be due to the enhanced intersystem crossing of **9a-b**, that results in the shortening of S1 lifetime. Also the iodo atom at the core position of the aza-BODIPYs **9a** and **9b** push the carbazole group out of plane to a major extent and does not allow taking part in direct conjugation with dipyrromethene ring which may reduce vibrations and thus the thermoelastic expansion in the molecule. The dyes **8a** and **8b**, which are free from the core substitution showed strong PAS signal when compared to blood. These can be attributed to their low intersystem crossing efficiency, which leads to an increase in the singlet excited state life time. The peak to peak PA signal amplitude for the sample **8a** in acetonitrile is found to be 198 times higher than that of blood (Figure 6B), and the signal intensity gets increased upon increasing the concentration of the sample. Therefore, the derivative, **8a** can be used as a promising photoacoustic contrast agent in deep tissue imaging.

Deep tissue photoacoustic imaging. To demonstrate the potential of the aza-BODIPY derivative, **8a** as a promising PA contrast agent, and to determine its imaging depth, a study was conducted to acquire the PA images of **8a** (in acetonitrile) and blood embedded inside chicken breast tissue (CBT). Two low density polyethylene (LDPE) tubes of 0.38 mm inner diameter were filled with blood and **8a** and placed on layer of CBT as shown in Figure 7A. PA data was acquired using a 2.25 MHz ultrasound transducer (UST) at various depths of ca. 1cm and ca. 2 cm by stacking layers of CBT one on top of the other (Figure 7B). Figures 7C and 7D show the reconstructed cross-sectional photoacoustic tomography (PAT) images at 1 cm and 2 cm depths, respectively. The signal-to-noise ratio (SNR) at ca. 1 cm depth for **8a** is measured to be 53.15 dB and for blood 29.63 dB. Notably at ca. 2 cm depth the SNR for **8a** is found to

be 42.23 dB whereas the blood tube was not visible at all. The PA signal for the aza-BODIPY derivative, **8a** is clearly seen even at the depth of 2 cm. Hence, the aza-BODIPY dye, **8a** can be used as a promising photoacoustic contrast agent that produces rich contrast during *in vitro* PAT imaging

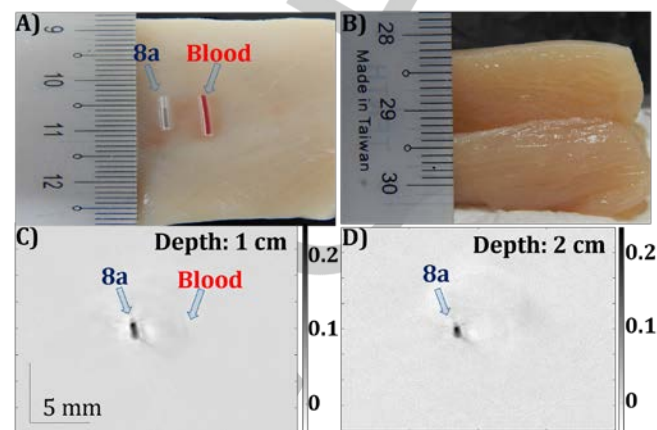


Figure 7. Deep tissue cross-sectional photoacoustic tomography (PAT) imaging of aza-BODIPY dye, **8a** and blood embedded inside chicken breast tissue using OPO-PAT system. (A) LDPE tubes filled with **8a** and blood. (B) Layers of chicken tissue in stacks inside which blood and **8a** were placed. (C) Cross-sectional PAT image at 1 cm depth. (D) Cross-sectional PAT image at 2 cm depth.

Conclusion

In conclusion, we have designed and synthesized four novel *N*-ethylcarbazole linked aza-BODIPY dyes and investigated their efficiency to produce triplet excited state and singlet oxygen generation. All these aza-BODIPY derivatives showed strong absorption in the NIR region with high molar extinction coefficients ($3\text{-}4 \times 10^4 \text{ M}^{-1}\text{cm}^{-1}$). The substitution of these derivatives with heavy atoms such as iodine at the core positions resulted in a significant enhancement in the intersystem crossing efficiency of **9a-b**. The triplet excited state quantum yields of ca. 90% and singlet oxygen generation efficiency of ca. 70% were observed for the core iodinated derivative **9a**. The orientation of carbazole group and the localisation of electron density in the molecule were confirmed from the optimised geometries through DFT calculations. Strong photoacoustic signal observed in the NIR region makes these molecules ideal for deep tissue contrast agent for photoacoustic imaging. Up to 2 cm deep photoacoustic imaging was successfully demonstrated by using **8a** as contrast agent. Our results demonstrate that these derivatives can have potential for theranostic application of simultaneous imaging and therapy by combining both photoacoustic imaging and photodynamic therapy.

1 Experimental Section

2 **General Techniques:** The melting points were determined on a
3 μ ThermoCal10 apparatus. The electronic absorption spectra were
4 recorded on a Shimadzu UV-3101 or 2401 PC UV-VIS-NIR scanning
5 spectrophotometer. The fluorescence spectra were recorded on a SPEX-
6 Fluorolog F112X spectrofluorimeter. ^1H , ^{13}C , ^{11}B and ^{19}F NMR (Fig. S1-
7 S22, Supporting Information) were recorded on a 500 MHz Agilent NMR
8 VNMRs spectrometer. Mass spectra were recorded on Bruker (maxis
9 impact), sr. no. 282001.00081. All the solvents used were purified and
10 distilled before use. Fluorescence quantum yields were measured by the
11 integration of the available area of fluorescence spectra by absolute
12 method using an integration sphere. Tris-(8-hydroxyquinoline)aluminum
13 (Alq_3) was used for the calibration of integration sphere before starting
14 the experiments.^[21]

15 **Quantification of triplet state properties:** The nanosecond laser flash
16 photolysis experiments were carried out by employing an Applied
17 Photophysics model LKS-20 laser kinetic spectrometer using OCR-122
18 Series Quanta Ray Nd:YAG laser. Laser beams were fixed at right
19 angles to each other. The laser energy was 64 mJ at 355 nm. The triplet
20 yields (Φ_T) of the synthesized aza-BODIPYs were measured employing
21 energy transfer to β -carotene using $\text{Ru}(\text{bpy})_3^{2+}$ as the reference.^[12] For
22 these experiments, an optically matched (355 nm) solutions of
23 $\text{Ru}(\text{bpy})_3^{2+}$ /aza-BODIPY derivatives were mixed with a known volume of
24 β -carotene solution (end concentration of β -carotene was 2.0×10^{-4} M).
25 The transient absorbance (ΔA) of the β -carotene triplet, formed by the
26 energy transfer from $\text{Ru}(\text{bpy})_3^{2+}$ or the aza-BODIPY triplet, was monitored
27 at 510 nm. The plateau absorbance following the completion of triplet
28 formation were compared and properly corrected for the decay of the
29 donor triplets in competition with energy transfer to β -carotene, and thus
30 calculated the Φ_T of aza-BODIPY derivatives based on eq. 1.

$$\Phi_T^{\text{bod}} = \Phi_T^{\text{ref}} \frac{\Delta A_{\text{bod}}}{\Delta A_{\text{ref}}} \frac{k_{\text{obs}}^{\text{bod}}}{k_{\text{obs}}^{\text{bod}} - k_0^{\text{bod}}} \frac{k_{\text{obs}}^{\text{ref}} - k_0^{\text{ref}}}{k_{\text{obs}}^{\text{ref}}} \dots \dots \dots (\text{eq. 1})$$

31 where superscripts 'bod' and 'ref' designate the different aza-BODIPY
32 derivatives and $\text{Ru}(\text{bpy})_3^{2+}$, respectively, k_{obs} is the pseudo-first-order
33 rate constant for the growth of the β -carotene triplet and k_0 is the rate
34 constant for the decay of the donor triplets, in the absence of β -carotene,
35 observed in solutions containing $\text{Ru}(\text{bpy})_3^{2+}$ or aza-BODIPY dye at the
36 same optical density (OD) as those used for sensitization. The direct
37 excitation of β -carotene did not result in any significant triplet formation
38 under these experimental conditions, because of negligible triplet yield.
39 The Φ_T^{ref} in methanol for $\text{Ru}(\text{bpy})_3^{2+}$ was taken to be unity. The Φ_T data
40 obtained in this manner are reliable to the extent to which the assumption
41 regarding 100% efficiency of energy transfer to β -carotene is valid.

43 **Quantification of singlet oxygen generation:** Singlet oxygen
44 generation studies were carried out with a light source 200 W mercury
45 lamp (model 3767) on an Oriel optical bench (model 11200) with a
46 grating monochromator (model 77250). The intensity of light was
47 maintained constant throughout the irradiations by measuring the output
48 using an Oriel photodiode detection system (model 7072). Quantum
49 yields for singlet oxygen generation in DMSO were determined by
50 monitoring the photooxidation of DPBF sensitized by the aza-BODIPY
51 derivatives. Singlet oxygen quantum yields were measured at low dye
52 concentrations (optical density 0.2-0.3 at the irradiation wavelength
53 >630 nm) to minimize the possibility of singlet oxygen quenching by the
54 dyes. The photooxidation of DPBF was monitored between 2 s to 2 min,
55 depending on the efficiency of the dye sensitizer. No thermal recovery of
56 DPBF (from a possible decomposition of endoperoxide product) was
57 observed under the conditions of these experiments. The quantum yields

of singlet oxygen generation ($\Phi[^1\text{O}_2]$) were calculated by a relative
method using optically matched solutions and comparing the quantum
yield of photooxidation of DPBF sensitized by the dye of interest to the
quantum yield of MB ($\Phi[^1\text{O}_2] = 52\%$) as the reference.^[14] The following eq.
2 was used,

$$\Phi_{\Delta}^{\text{bod}} = \Phi_{\Delta}^{\text{MB}} \frac{m^{\text{bod}} F^{\text{MB}}}{m^{\text{MB}} F^{\text{bod}}} \dots \dots \dots (\text{eq. 2})$$

where superscripts 'bod' and 'MB' designate aza-BODIPY derivatives
and MB, respectively, Φ_{Δ} is the quantum yield of singlet oxygen, 'm' is
the slope of a plot of difference in change in absorbance of DPBF (at 418
nm) with the irradiation time and 'F' is the absorption correction factor,
which is given by $F = 1 - 10^{-\text{OD}}$ (OD at the irradiation wavelength).

Photoacoustic imaging system: Each sample was injected into a
transparent LDPE tube of 0.38 mm inner diameter and was irradiated
with Optical Parametric Oscillator (OPO) laser (Continuum, Surelite)
pumped with 10 Hz repetition rate Q-switched Nd:YAG laser maintaining
5 ns pulse width and pulse energy density of ~ 5 -10 mJ/cm². The laser
irradiation results in thermoelastic expansion of the sample which in turn
generates PA waves. These PA waves are detected using a single-
element UST (Olympus NDT, V306-SU) of 2.25 MHz central frequency
with $\sim 70\%$ nominal bandwidth. The UST and the LDPE tubes were
enclosed in a water bath for better acoustic coupling. The acquired PA
signal was first amplified and band pass filtered (1-10 MHz) using a pulse
amplifier (Olympus-NDT, 5072PR) and then recorded using a data
acquisition card (GaGe, compuscope 4227) inside a desktop. All PA
signals were acquired with a sampling rate of 25 MHz. The laser
wavelength was varied from 670-970 nm with step size of 5 nm. Each PA
signal was averaged 10 times and normalised with laser power and
amplifier gain. For deep tissue imaging experiments, we have used the
OPO-PAT system (Fig 1. in ^[19]). The PA signal was acquired by rotating
the UST continuously in a full 360^o around the sample. The acquired PA
data was then amplified and filtered. A simple delay-and-sum
reconstruction algorithm was used to obtain the PAT images^[20]. SNR of
the PAT images were calculated as the ratio of peak-to-peak amplitude
of the PA signal (V) to the standard deviation of background noise (n) i.e.,
 $\text{SNR (in dB)} = 20 \log_{10} (V/n)$.

Materials and Methods: The starting materials, carbazole,
acetophenone, 4-bromoacetophenone, ethyl iodide, nitromethane,
diethylamine, ammonium acetate, borontrifluoride diethyl etherate,
triethylamine, *N*-iodosuccinimide, methylene blue, 1,3-
diphenylisobenzofuran, β -carotene were purchased from S. D. Fine and
sigma Aldrich Chemicals, India. 1,3-diphenylisobenzofuran (DPBF) was
recrystallized from a mixture (1:1) of ethanol and chloroform. The
compounds **2** (mp: 71-73^oC) and **3** (mp: 85-87^oC) were synthesized in
good yields by following the literature reported procedures.^[22]

General procedure for the synthesis of 5a-b

5a-b were synthesized by modifying the reported procedures^[22a, 23], 9-
ethyl-9H-carbazole-3-carbaldehyde, **2** (0.022 mol) and acetophenone
derivatives **3a-b** (0.022 mol) were dissolved in methanol (300 mL) and
2.5 molar aq.KOH (150 ml) added dropwise while cooling. After the
complete addition, reaction mixture allowed to stir for 24 h. The
precipitated product was filtered, washed with cold methanol, dried and
recrystallized from ethanol to give **5a-b** as yellow solid.

5a: 63%, mp 67-69 $^{\circ}\text{C}$; ^1H NMR (500 MHz, CDCl_3) δ 8.17 (m, 1H), 8.04
(d, J = 7.5 Hz, 1H), 7.92 (d, J = 8.0 Hz, 2H), 7.53 – 7.49 (m, 2H), 7.39-
7.36 (dd, J=8.2 1H), 7.18 – 7.10 (m, 4H), 7.06-7.04 (m, 2H), 7.00 (d, 1H),

- 1 4.25 (q, $J=7.2$ Hz, 2H), 1.14 (t, $J = 7.1$ Hz, 3H). ^{13}C NMR (125 MHz, CDCl_3) 189.04, 146.50, 142.34, 140.83, 139.57, 135.92, 130.28, 125.65, 124.31, 122.67, 121.04, 119.8, 118.4, 113.08, 111.44, 110.47, 109.50, 108.60, 47.10, 38.80, 15.19 cm^{-1} ; ESI-MS m/z Cald for $\text{C}_{23}\text{H}_{19}\text{NO}$ 325.147, Found 326.14.
- 6 **5b**: 58%, mp 125-127 °C; ^1H NMR (500 MHz, CDCl_3) δ 8.38 (s, 1H), 8.18 (d, $J = 7.6$ Hz, 1H), 8.06 (d, $J = 15.5$ Hz, 1H), 7.94 (d, $J = 8.4$ Hz, 2H), 7.79 (d, $J = 8.5$ Hz, 1H), 7.66 (d, $J = 8.4$ Hz, 2H), 7.53 (dd, $J = 15.3$, 6.0 Hz, 2H), 7.46 – 7.41 (m, 2H), 7.30 (m, 1H), 4.40 (q, $J = 7.3$ Hz, 2H), 1.47 (t, $J = 7.2$ Hz, 3H). ^{13}C NMR (126 MHz, CDCl_3) δ : 189.46, 147.13, 141.59, 140.51, 137.52, 131.84, 129.98, 127.40, 125.70, 123.51, 122.78, 121.76, 120.67, 119.82, 118.38, 109.13, 108.93, 108.17, 37.81, 13.85 cm^{-1} ; ESI-MS m/z Cald for $\text{C}_{23}\text{H}_{18}\text{BrNO}$ 403.057, Found 404.06.
- 14 *General procedure for the synthesis of 6a-b*
- 15 **6a-b** were synthesized by modifying the reported procedures [24, 3a]. To a solution of **5a-b** (0.02 mol) dissolved in 100 mL of methanol was added diethyl amine (9 mL) and nitromethane (4.5 mL) and refluxed for 24 h. The mixture was cooled and neutralized using 1N HCl and extracted with chloroform. The removal of the solvent gave a residue which was separated by column chromatography over silica gel. Elution of the column with a mixture (1:9) of ethyl acetate and hexane gave **6a-b** in good yields.
- 23 **6a**: 69%, Viscous liquid; ^1H NMR (500 MHz, CDCl_3) δ 8.46 (m, $J = 8.4$ Hz, 2H), 7.97 (m, 1H), 7.82 (m, 1H), 7.69 (m, 2H), 7.62 (m, 1H), 7.46 (m, 2H), 7.29 (m, 2H), 7.08 (m, 1H) 4.87 (m, 2H), 4.75 (m, 2H), 4.19 (m, 1H), 2.97 (d, 2H), 1.44 (t, $J = 7.2$ Hz, 3H); ^{13}C NMR (126 MHz, CDCl_3) δ : 196.56, 163.41, 139.21, 137.72, 133.50, 131.67, 129.51, 129.09, 127.89, 126.93, 125.15, 124.78, 122.78, 121.04, 118.19, 118.08, 80.46, 42.21, 39.46, 37.56, 36.51, 31.3, 30.48, 13.76; ESI-MS m/z Cald for $\text{C}_{24}\text{H}_{22}\text{N}_2\text{O}$ 386.163, Found 387.1.
- 31 **6b**: 80%, m.p. 69-71 °C; ^1H NMR (500 MHz, CDCl_3) δ 8.03 (dd, $J = 7.2$ Hz, 2H), 7.69 (dd, $J = 8.6$ Hz, 2H), 7.47 (m, 1H), 7.39 (m, 1H), 7.29 (m, 2H), 7.08 (m, 1H), 4.80 (m, 1H), 4.41 (m, 2H), 3.56 (m, 2H), 2.92 (d, 2H), 1.42 (t, $J = 7.2$ Hz, 3H); ^{13}C NMR (126 MHz, CDCl_3) δ 196.34, 163.98, 140.28, 139.40, 135.30, 132.06, 129.54, 129.04, 128.70, 126.01, 124.88, 123.30, 122.41, 120.46, 119.15, 118.95, 80.42, 42.19, 39.55, 37.60, 36.47, 31.42, 30.48, 13.83; ESI-MS m/z Cald for $\text{C}_{24}\text{H}_{21}\text{BrN}_2\text{O}_3$ 464.079, Found 465.0.
- 39 *General Procedure for the synthesis of 7a-b*
- 40 The nitromethane derivatives **6a-b** (0.01 mol) and ammonium acetate (27.30 g, 0.314 mol) were dissolved in butanol (60 mL) and heated under reflux for 24 h. [15c] The precipitated product was filtered, washed with cold ethanol, dried and recrystallized from chloroform to give **7a-b** as brown solid.
- 45 **7a**: 57%, m.p. 225-227 °C; ^1H NMR (500 MHz, CDCl_3) δ 8.84 (s, 2H), 8.33 (d, $J = 8.5$ Hz, 2H), 8.02 (d, $J = 7.3$ Hz, 4H), 7.86 (d, $J = 7.6$ Hz, 2H), 7.55 (t, $J = 7.6$ Hz, 4H), 7.47 (t, $J = 7.3$ Hz, 2H), 7.39 (m, 4H), 7.31 (d, $J = 8.5$ Hz, 2H), 7.27 (s, 2H), 7.01 (t, $J = 7.3$ Hz, 2H), 4.27 (q, $J = 7.2$ Hz, 4H), 1.38 (t, $J = 7.2$ Hz, 6H); ^{13}C NMR (126 MHz, CDCl_3) δ 154.79, 149.89, 143.80, 140.26, 139.83, 132.57, 129.70, 129.04, 127.21, 126.51, 125.47, 125.20, 123.36, 123.20, 121.48, 120.77, 118.71, 113.37, 108.52, 108.59, 77.24, 76.99, 76.74, 37.58, 13.87; ESI-MS m/z Cald for $\text{C}_{48}\text{H}_{37}\text{N}_5$ 683.305, Found 684.312.
- 7b: 66%, m.p. 272-274 °C; ^1H NMR (500 MHz, CDCl_3) δ 8.58 (s, 2H), 8.13 (d, $J = 7.6$ Hz, 2H), 8.10 (d, $J = 7.8$ Hz, 4H), 7.50 (d, $J = 7.3$ Hz, 2H), 7.46 (m, 4H), 7.43 (d, 2H), 7.42 – 7.39 (m, 4H), 7.35 (m, 2H), 7.26 (s, 1H), 7.19 (t, $J = 7.4$ Hz, 2H), 4.31 (q, $J = 7.3$ Hz, 4H), 1.46 (t, $J = 7.3$ Hz, 6H). ^{13}C NMR (126 MHz, CDCl_3) δ 154.76, 149.49, 141.50, 140.97, 140.47, 134.18, 128.98, 128.11, 127.51, 126.16, 124.62, 123.59, 123.35, 123.01, 120.64, 119.47, 118.86, 114.09, 108.95, 108.86, 37.70, 13.89; ESI-MS m/z Cald for $\text{C}_{48}\text{H}_{35}\text{Br}_2\text{N}_5$ 841.124, Found 842.0.
- General procedure for the synthesis of 8a-b*
- 8a-b** were synthesized by modifying the reported procedures. [25, 15c] Compounds **7a-b** (0.62 mmol) dissolved in dry dichloromethane (100 mL) was treated with triethylamine (1.14 mL, 8.1 mmol) and stirred for 10 min at 30 °C. To this reaction mixture, boron trifluoride diethyl etherate (4.65 mL, 13.1 mmol) was added and heated at 40 °C for 5 h. The solvent was evaporated, washed with water (2 x 50 mL) and extracted with chloroform. Removal of the solvent gave a residue, which was separated by column chromatography over silica gel. Elution of the column with a mixture (1:9) of ethyl acetate and hexane gave the products **8a-b** as metallic blue solid.
- 8a**: 34%, m.p. 234-236 °C; ^1H NMR (500 MHz, DMSO) δ 9.06 (s, 2H), 8.47 (d, $J = 8.7$ Hz, 2H), 8.12 (m, 4H), 8.07 (d, $J = 7.7$ Hz, 2H), 7.66 (m, 6H), 7.57 (m, 6H), 7.47 (m, 2H), 7.12 (m, 2H), 4.44 (m, 4H), 1.31 (t, $J = 7.1$ Hz, 6H). ^{13}C NMR (126 MHz, DMSO) δ 158.59, 145.78, 145.01, 140.76, 140.42, 132.18, 130.38, 129.49, 128.45, 128.00, 127.44, 126.03, 124.03, 123.64, 123.32, 122.21, 120.88, 119.25, 117.18, 108.97, 108.73, 37.74, 13.95. ^{19}F NMR (160 MHz, DMSO) δ 1.22, 1.02, 0.83. ^{19}F NMR (470 MHz, DMSO) δ -128.40, -128.47, -128.54, -128.61; ESI-MS m/z Cald for $\text{C}_{48}\text{H}_{36}\text{BF}_2\text{N}_5$ 731.303, Found 732.310.
- 8b**: 41%, m.p. 289-291 °C; ^1H NMR (500 MHz, DMSO) δ 9.06 (d, 2H), 8.47 (d, $J = 8.5$ Hz, 2H), 8.30 (s, 2H), 8.04 (m, 6H), 7.79 (m, 3H), 7.68 (m, 4H), 7.48 (m, 3H), 7.12 (m, 2H), 4.45 (m, 4H), 1.31 (d, $J = 7.2$ Hz, 6H); ^{13}C NMR (126 MHz, DMSO) δ 158.40, 145.46, 145.03, 140.94, 140.55, 131.89, 131.29, 129.80, 129.07, 127.80, 126.81, 123.66, 123.39, 122.88, 122.56, 121.02, 119.85, 118.57, 110.13, 37.69, 14.33. ^{19}F NMR (470 MHz, DMSO) δ -128.28, -128.34, -128.41, -128.48; ESI-MS m/z Cald for $\text{C}_{48}\text{H}_{34}\text{BBr}_2\text{F}_2\text{N}_5$ 889.122, Found 890.130.
- General procedure for the synthesis of 9a-b*
- To a solution of **8a-b** (0.27 mmol) in a mixture (60 mL, 3:1) of chloroform and acetic acid, *N*-iodosuccinimide (154 mg, 0.68 mmol) was added and stirred at 30 °C for 2 h. The reaction mixture was washed with sodium thiosulphate followed by sodium bicarbonate solution and extracted with chloroform. Removal of the solvent gave a residue which was separated by column chromatography over silica gel. Elution of the column with a mixture (1:9) of methanol and chloroform gave 60-65% of **9a-b**.
- 9a**: 61%, m.p. >300 °C; ^1H NMR (500 MHz, DMSO) δ 8.69 (d, 2H), 8.61 (m, 2H), 8.14 (m, 2H), 8.08 (d, $J = 8.4$ Hz, 1H), 7.97 (d, $J = 9.0$ Hz, 1H), 7.76 (m, 2H), 7.59 (m, 4H), 7.53 (m, 6H), 7.48 (m, 2H), 7.43 (m, 2H), 4.30 (m, 4H), 1.06 (t, $J = 7.1$ Hz, 6H); ^{13}C NMR (126 MHz, DMSO) δ 158.40, 145.46, 145.03, 140.94, 140.55, 131.89, 131.29, 129.80, 129.07, 127.80, 126.81, 123.66, 123.39, 122.88, 122.56, 121.02, 119.85, 118.57, 110.13, 37.69, 14.33; ^{19}F NMR (470 MHz, DMSO) δ -130.01, -130.08, -130.13, -130.18; ESI-MS m/z Cald for $\text{C}_{48}\text{H}_{34}\text{BF}_2\text{I}_2\text{N}_5$ 983.096, Found 984.033.
- 9b**: 58%, m.p. >300 °C; ^1H NMR (500 MHz, CDCl_3) δ 8.59 (s, 1H), 8.53 (s, 1H), 8.48 (s, 1H), 8.17 (d, 2H), 8.10 – 8.08 (m, 2H), 7.85 (m, 1H), 7.77

(m, 1H), 7.66 (m, 1H), 7.59 (m, 6H), 7.30 (m, 4H), 7.05 (m, 2H), 4.15 (m, 4H), 0.85 (s, 6H). ¹¹B NMR (160 MHz, CDCl₃) δ 0.38, 0.23, 0.03. ¹³C NMR (470 MHz, CDCl₃) δ -131.69, -131.75, -131.81, -131.87; ESI-MS m/z Calcd for C₄₈H₃₂BBR₂F₂N₅, 1140.915, Found 1141.925.

6 Acknowledgements

The authors Y. G. and N. S. greatly thankful to University Grant Commission-SAP, New Delhi, India for providing financial support. The authors N. A, J. J and D. R acknowledge the financial support from CSIR(CSC0134&NWP55), and Department of Science and Technology, Government of India. Author M. P. Acknowledges the financial support by the Tier 1 grant funded by the Ministry of Education in Singapore (RG41/14: M4011285, RG48/16: M4011617), and the Singapore Ministry of Health's National Medical Research Council (NMRC/OFIRG/0005/2016: M4062012). Authors have no relevant financial interests in the manuscript and no other potential conflicts of interest to disclose.

Keywords: Aza-BODIPY • Dyes and pigments • Triplet excited state • Singlet oxygen • Photoacoustic spectra

21 References

- [1] a) S. Toyokuni, *Pathol. Int.* **1999**, *49*, 91–102; b) S. G. Awuah, You, *RSC Adv.* **2012**, *2*, 11169.
- [2] a) C. Schweitzer, R. Schmidt, *Chem. Rev.* **2003**, *103*, 1685–1757; b) E. S. Nyman, H. Hynninen, *J. Photochem. Photobiol. B* **2004**, *73*, 28; c) I. S. Turan, D. Yildiz, A. Turkoys, G. Gunaydin, E. U. Akkaya, *Angew. Chem. Int. Ed.* **2016**, *55*, 2875–2878; d) S. D. Topel, G. Cin, E. U. Akkaya, *Chem. Commun.* **2014**, *50*, 8896–8899.
- [3] a) N. Adarsh, M. Shanmugasundaram, R. R. Avirah, D. Ramaiah, *Chem. Eur. J.* **2012**, *18*, 12655–12662; b) V. S. Thoi, J. R. Stork, D. Magde, S. M. Cohen, *Inorg. Chem.* **2006**, *45*, 10688–10697; c) I. S. Turan, F. P. Cakmak, D. C. Yildirim, R. Cetin-Atalay, E. U. Akkaya, *Chem. Eur. J.* **2014**, *20*, 16088–16092.
- [4] a) T. Matsubara, K. Kusuzaki, A. Matsumine, H. Satonaka, K. Shintani, T. Nakamura, A. Uchida, *In Vivo.* **2008**, *22*, 297–304; b) W. Lin, J. R. Shulok, S. D. Kirley, C. M. Bachelder, T. J. Flotte, M. E. Sherwood, L. Cincotta, J. W. Foley, *Photochem. Photobiol.* **1993**, *58*, 81–91; c) C. W. Lin, J. R. Shulok, S. D. Kirley, L. Cincotta, J. W. Foley, *Cancer Res.* **1991**, *51*, 2710–2719; d) R. Danaboyina, A. Joy, N. Chandrasekhar, N. V. Eldho, S. Das, M. V. George, *Photochem. Photobiol.* **1997**, *65*, 783–790; e) K. Jyothish, R. R. Avirah, D. Ramaiah, *Org. Lett.* **2006**, *8*, 111–114; f) R. R. Avirah, D. Jayaram, N. Adarsh, D. Ramaiah, *Org. Biomol. Chem.* **2012**, *10*, 911.
- [5] a) P. Agostinis, K. Berg, K. A. Cengel, T. H. Foster, A. W. Girotti, S. O. Gollnick, S. M. Hahn, M. R. Hamblin, A. Juzeniene, D. Kessel, *Am. Cancer Soc.* **2011**, *61*, 250–281; b) S. Erbas-Cakmak, F. Cakmak, S. D. Topel, T. B. Uyar, E. U. Akkaya, *Chem. Commun.* **2015**, *51*, 12258–61.
- [6] a) A. Kamkaew, S. H. Lim, H. B. Lee, L. V. Kiew, L. Y. Chung, Burgess, *Chem. Soc. Rev.* **2013**, *42*, 77–88; b) T. Yogo, Y. Urano, Ishitsuka, F. Maniwa, T. Nagano, *J. Am. Chem. Soc.* **2005**, *127*, 12162–12163; c) P. Batat, M. Cantuel, G. Jonusauskas, Scarpantonio, A. Palma, D. F. O'Shea, N. D. McClenaghan, *J. Phys. Chem. A* **2011**, *115*, 14034–14039. d) N. Adarsh, R. R. Avirah, D. Ramaiah, *Org. Lett.* **2010**, *12*, 5720–5723; e) J. K. G. Karlsson, Harriman, *J. Phys. Chem. A* **2016**, *120*, 2537–2546; f) A. Nano, Retailleau, J. P. Hagon, A. Harriman, R. Ziessel, *Phys. Chem. Chem. Phys.* **2014**, *16*, 10187–98; g) R. Misra, T. Jadhav, B. Dhokale, P. Gautam, R. Sharma, R. Maragani, S. M. Mobin, *Dalt. Trans.* **2014**, *43*, 13076; h) A. Harriman, P. Stachelek, A. Sutter, R. Ziessel, D. Beljonne, C. Curutchet, G. D. Scholes, R. J. Silbey, J. S. Wu, W. M. Liu, et al., *Photochem. Photobiol. Sci.* **2015**, *14*, 1100–1109.
- [7] a) W. M. Gallagher, L. T. Allen, C. O'Shea, T. Kenna, M. J. Hall, J. Killoran, D. F. O'Shea, *Br. J. Cancer* **2005**, *92*, 1702–1710; b) A. T. Byrne, A. E. O'Connor, M. Hall, J. Murtagh, K. O'Neill, K. M. Curran, K. Mongrain, J. A. Rousseau, R. Lecomte, S. McGee, J. J. Callanan, D. F. O'Shea, W. M. Gallagher, *Br. J. Cancer* **2009**, *101*, 1565–1573; c) J. Joseph, N. V. Eldho, D. Ramaiah, *Chem. Eur. J.* **2003**, *9*, 5926–5935; d) S. Kumar, T. K. Khan, M. Ravikanth, *Tetrahedron* **2015**, *71*, 7608–7613; e) A. Dvivedi, S. Kumar, M. Ravikanth, *Sens. Actuators, B.* **2016**, *224*, 364–371; f) S. Kumar, H. B. Gobeze, T. Chatterjee, F. D'Souza, M. Ravikanth, *J. Phys. Chem. A* **2015**, *119*, 8338–8348; g) R. Sharma, H. B. Gobeze, F. D'Souza, M. Ravikanth, *ChemPhysChem* **2016**, *5017*, 2516–2524; h) T. Jadhav, R. Misra, S. Biswas, G. D. Sharma, *Phys. Chem. Chem. Phys.* **2015**, *17*, 26580–26588; i) N. Balsukuri, M. Y. Lone, P. C. Jha, S. Mori, I. Gupta, *Chem. Asian J.* **2016**, *11*, 1572–1587.
- [8] S. Huang, P. K. Upputuri, H. Liu, M. Pramanik, M. Wang, *J. Mater. Chem. B* **2016**, *4*, 1696–1703.
- [9] a) L. V. Wang, S. Hu, *Science* **2012**, *335*, 1458–1462; b) L. V. Wang, J. Yao, *Nat. Methods.* **2016**, *13*, 627–638. c) W. Xia, D. Piras, M. K. A. Singh, J. C. G. van Hespren, T. G. van Leeuwen, W. Steenbergen, S. Manohar, *Biomed. Opt. Express* **2013**, *4*, 2555–69; d) C. Kim, J. A. Margenthaler, M. D. Pashley, L. V. Wang, *radiology* **2010**, *256*, 102–110; e) M. Pramanik, G. Ku, C. Li, L. V. Wang, *Med. Phys.* **2008**, *35*, 2218–2223. e) X. Cai, C. Kim, M. Pramanik, L. V. Wang, *J. Biomed. Opt.* **2011**, *16*, 46017.
- [10] a) D. Pan, M. Pramanik, A. Senpan, J. S. Allen, H. Zhang, S. a Wickline, L. V. Wang, G. M. Lanza, *The FASEB J.* **2011**, *25*, 875–882; b) M. Pramanik, K. H. Song, M. Swierczewska, D. Green, B. Sitharaman, L. V. Wang, *Phys. Med. Biol.* **2009**, *54*, 3291–301; c) A. De la Zerda, C. Zavaleta, S. Keren, S. Vaithilingam, S. Bodapati, Z. Liu, J. Levi, B. R. Smith, T.-J. Ma, O. Oralkan, Z. Cheng, X. Chen, H. Dai, B. T. Khuri-Yakub, and S. S. Gambhir, *Nat. Nanotechnol.* **2008**, *3*(9), 557–562; d) C. Kim, C. Favazza, and L. V. Wang, *Chem. Rev.* **2010**, *110*(5), 2756–2782; e) K. Sivasubramanian, M. Mathiyazhakan, C. Wiraja, P. K. Upputuri, C. Xu, and M. Pramanik, *J. Biomed. Opt.* **2017** *22* (4), (In Press); f) Y. Toumia, F. Domenici, S. Orlanducci, F. Mura, D. Grishenkov, P. Trochet, S. Lacerenza, F. Bordin, and G. Paradossi, *ACS Appl. Mater. Interfaces* **2016**, *8*, (25) 16465. g) Y. Shi, D. Peng, K. Wang, X. Chai, Q. Ren, J. Tian, and C. Zhou, *Biomed. Opt. Express* **2017**, *7*, 1830–1841; h) C. Gao, Z.-J. Deng, D. Peng, Y.-S. Jin, Y. Ma, Y.-Y. Li, Y.-K. Zhu, J.-Z. Xi, J. Tian, and Z.-F. Dai, *Cancer Biology & Medicine* **2016**, *13* (3), 349–359; i) K. Pu, A. J. Shuhendler, J. V. Jakerst, J. Mei, S. S. Gambhir, Z. Bao, and J. Rao, *Nat. Nanotechnol.* **2014** *9* (3), 233–239.
- [11] a) D. Ramaiah, A. Joy, N. Chandrasekhar, N. V. Eldho, S. Das, M. V. George, *Photochem. Photobiol.* **1997**, *65*, 783–790.
- [12] a) V. S. Jisha, K. T. Arun, M. Hariharan, D. Ramaiah, *J. Phys. Chem. B* **2010**, *114*, 5912–5919.
- [13] M. Mirenda, C. A. Strassert, L. E. Dicello, San Roman E. *ACS Appl. Mater. Interfaces* **2010**, *2*, 1556–1560.
- [14] a) P. R. Ogilby, C. S. Foote, *J. Am. Chem. Soc.* **1983**, *105*, 3423–3430; b) M. Nemoto, H. Kokubun, M. Koizumi, *Bull. Chem. Soc.* **1969**, *42*, 1223–1228.
- [15] a) R. R. Gagne, C. A. Koval, G. C. Lisensky, *Inorg. Chem.* **1980**, *19*, 2854–2855; b) P. E. Kesavan, I. Gupta, *Dalt. Trans.* **2014**, *43*, 12405–12413; c) A. Gorman, J. Killoran, C. O'Shea, T. Kenna, W. M. Gallagher, D. F. O'Shea, *J. Am. Chem. Soc.* **2004**, *126*, 10619–10631.
- [16] L. Le Bahers, C. Adamo, F. Odobel, D. Jacquemin, *J. Phys. Chem. C* **2012**, *116*, 11946–11955.
- [17] M. D. Kasha, *Faraday Soc.* **1950**, *9*, 14–19.
- [18] M. Frenette, M. Hatamimoslehabadi, S. Bellinger-buckley, S. Laoui, J. La, S. Bag, S. Mallidi, T. Hasan, B. Bouma, C. Yelleswarapu, J. Rochford, *J. Am. Chem. Soc.* **2014**, *136*, 15853–15856.
- [19] P. K. Upputuri, and M. Pramanik, *Biomedical Optics Express*, **2015** *6* (10), 4118–4129.
- [20] S. K. Kalva, and M. Pramanik, *J. Biomed. Opt.* **2016** *21* (8), 086011.
- [21] L. D. Carlos, C. De Mello Donegá, R. Q. Albuquerque, S. Alves, J. F. S. Menezes, O. L. Malta, *Mol. Phys.* **2003**, *101*, 1037–1045.
- [22] a) G. Bai, J. Li, D. Li, C. Dong, X. Han, P. Lin, *Dye. Pigment.* **2007**, *75*, 93–98. b) K. G. Thorat, P. Kambale, A. K. Ray, N. Sekar, *Phys. Chem. Chem. Phys.* **2015**, *17*, 17221–17236.
- [23] V. D. Gupta, V. S. Padalkar, K. R. Phatangare, V. S. Patil, P. G. Umape, N. Sekar, *Dye. Pigment* **2011**, *88*, 378–384.
- [24] S. C. Lee, D. Zhai, P. Mukherjee, Y. T. Chang, *Mater.* **2013**, *6*, 1779–1788.

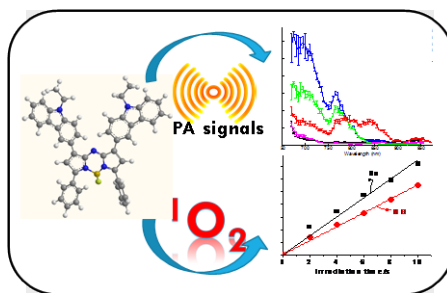
[25] P. A. Bouit, K. Kamada, P. Fenevrou, G. Berginc, L. Toupet, O.2

Maury, C. Andraud, *ADV MATER* 2009, 21, 1151–1154.

Table of Contents

FULL PAPER

The carbazole linked aza-BODIPY dyes showed favorable photophysical properties and efficient triplet as well as singlet oxygen generation quantum yields. Furthermore, the efficient photoacoustic signals produced by these dyes makes them as excellent candidates for both photodynamic therapy and contrast agents for photoacoustic imaging.



Y. Gawale, N. Adarsh, S. K. Kalva, J. Joseph, M. Pramanik, D. Ramaiah^{*} and N. Sekar^{*}

XXXXX – XXXXX

Carbazole Linked NIR Aza-BODIPY Dyes as Triplet Sensitizers and Photoacoustic Contrast Agents for Deep Tissue Imaging